Journal of Energy Storage 99 (2024) 113324

Contents lists available at ScienceDirect

Journal of Energy Storage

journal homepage: www.elsevier.com/locate/est

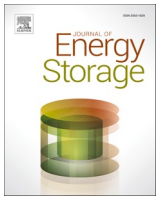

Research papers

Design of solar and energy storage systems fed reduced switch multilevel converter with flower pollination optimization

Koganti Srilakshmi [a], Amit Kumar [b,*], Krishnaveni Kondreddi [c], T. Murali Krishna [c], Praveen Kumar Balachandran [d,e,*], Gianluca Gatto [b]

[a] Department of Electrical and Electronics Engineering, Sreenidhi Institute of Science & Technology, Hyderabad, Telangana 501301, India
[b] Department of Electrical and Electronic Engineering, University of Cagliari, Via Marengo 2, Cagliari 09123, Italy
[c] Department of Electrical and Electronics Engineering, Chaitanya Bharathi Institute of Technology, Telangana 500075, India
[d] Department of Electrical, Electronic and Systems, Faculty of Engineering and Built Environment, Universiti Kebangsaan Malaysia, Selangor, Malaysia
[e] Department of Electrical and Electronics Engineering, Vardhaman college of Engineering, Hyderabad, Telangana, India

ARTICLE INFO

Keywords:
PID controller
Flower pollination optimization algorithm
Energy Storage System
Solar Energy System
Shunt active power filter

ABSTRACT

In the present situation, the growing use of power electronic devices and non-linear loads has led to power quality (PQ) issues, including harmonics and poor power factor, which adversely affect the distribution network. This study contributes a design of shunt active power filter, powered by solar energy and energy storage systems, to address these PQ issues. To minimize losses, a five-level reduced-switch voltage source converter has been considered. Additionally, a neural network-based reference signal generation method is used, eliminating the need for conventional synchronous reference frame and active-reactive power theories, along with their complex abc and αβ0 transformations. This work also includes the optimal selection of the shunt filter and the gain parameters for the proportional-integral-derivative (PID) controller used in the shunt and battery control system. These parameters, along with the weights and biases of the neural network, are optimally determined using a nature-inspired flower pollination optimization algorithm.

The proposed system has three primary objectives: (1) stabilizing the voltage across the DC bus capacitor, (2) reducing total harmonic distortion (THD) and improving the power factor (PF), and (3) ensuring the power management under the varying irradiation and load conditions. The effectiveness of the proposed system is evaluated through three testing scenarios, with results compared to conventional SRF and pq methods using a proportional-integral controller (PIC). The analysis reveals that the THD for the case studies is 3.32 %, 2.93 %, and 3.98 %, significantly lower than the other techniques compared. Additionally, the PF is nearly at unity, with a lower settling time of 0.05 s for the DC bus voltage.

1. Introduction

In recent years, there has been a drive to encourage the integration of clean energy sources, including wind and solar energy, into the electric distribution system. This is done to reduce the burden on the voltage sourced converters. The term “reduced switch” means achieving goals with fewer switches than traditional systems. However, the decreased switches can result in advantages like decreased expenses, energy wastage, and enhanced dependability. Reduced switch shunt active power filter (SHAPF), similar to other active power filters, has a vital function in preserving a steady and superior power provision in distribution network.

1.1. Motivation

The SHAPF powered by alternative energy sources has gained significant importance in solving power quality (PQ) issues with the multilevel voltage source converter (VSC). However, with the conventional multilevel VSC, the number of switches required is high, which leads to higher switching losses. On the other hand, most of the research in the past years involves only traditional methods like synchronous reference frame (SRF) and active-reactive power (pq) theories with

* Corresponding authors.
E-mail addresses: amit.kumar@unica.it (A. Kumar), krishnaveni_eee@cbit.ac.in (K. Kondreddi), tmuralikrishna_eee@cbit.ac.in (T.M. Krishna), gatto@unica.it (G. Gatto).

https://doi.org/10.1016/j.est.2024.113324
Received 21 May 2024; Received in revised form 2 August 2024; Accepted 10 August 2024
Available online 19 August 2024

Table 1
Literature survey.

Reference number	Technique adopted for		PQ Issues		Loads		Renewable sources	Multi-Level VSC	Optimization algorithm
	VSC Ref signal production	Filter Controller	THD	DC bus regulation	Balanced sensitive	Unbalanced Harmonics	Solar/ Wind	Reduced switch	Parameters and controller
[4]	p-q theory	FLC-SMC	✓	✓	✓	✓	✓		
[5]	SRF theory	NN-SMC	✓	✓	✓		✓		
[7]	p-q theory	FLC-NN	✓	✓	✓	✓	✓		
[14]	SRF theory	NN	✓	✓	✓	✓	✓		
[16]	NN	ANFIS	✓		✓	✓	✓		✓
[17]	NN	ANFIS	✓	✓	✓	✓	✓		✓
[28]	SRF theory	FOPIDC	✓	✓	✓	✓	✓		
[29]	SRF theory	FLC-PI	✓		✓	✓	✓		
Developed method	NN	Optimized PID	✓	✓	✓	✓	✓	✓	✓

complex abc, αβ transformations in combination with PIC, and sliding mode controller (SMC) techniques applied to different types of loads without any suitable selection of filter parameters or controller parameters of storage battery system and power management. Nevertheless, these approaches have failed to achieve optimal values when there are variations in sun irradiation and load demand.

1.2. Literature

A unique automatic transition method was introduced for the Photovoltaic (PV) and battery associated unified power quality conditioner (UPQC) to tackle PQ concerns in both grid and islanded approaches efficiently. Furthermore, the system's functionality was confirmed by empirical data [1]. Moreover, AI control techniques were implemented to tackle PQ issues that were resolved by a multilevel converter-based UPQC [2,3]. The AI based hybrid approaches in association to the standard methods like SMC, PI with self tuning filter was suggested to address the PQ issues under different loading conditions [4–6]. Additionally, the sport-based soccer league player algorithm was strategically utilized to select the gains of the PI control system, a crucial step in effectively addressing PQ issues [7]. On a different note, football optimization was selected for the optimal determination of filter parameters for the H-bridge five-level UPQC [8].

The UPQC device, in conjunction with PV and storage system, was proposed as a remedy to alleviate THD and address issues with grid voltage [9]. Besides, the versatile control technique was developed for the UPQC and was examined on different control algorithms to enhance PQ [10]. Next, the most valuable player optimization was selected to determine the gains of the PID control system with the objective of addressing PQ issues [11]. Meanwhile, using the feed-forward method, a neural network (NN) controller was used for a UPQC coupled to both solar and wind energy sources. The mentioned controller was employed to regulate the voltage and control the reactive power within the grid [12].

Furthermore, the Jaya-Grey Wolf hybrid algorithm was used to optimize the fractional-order PID controller for a hybrid active power filter with a renewable source, incorporating a three-level VSC to enhance PQ [13]. Similarly, a firefly algorithm was selected to train the NN controller for the shunt active filter integrated with green energy sources to improve PQ [14]. Meanwhile, the golden ball optimization algorithm was selected to optimize the FLC of the SHAPF powered by non-conventional energy sources to address PQ issues [15]. The enhanced harmony search with the predator-prey algorithm was developed to optimize the ANFIS control system of the UPQC for solving PQ problems [16]. Next, the combination of the firefly algorithm with harmony search was introduced to optimize the ANFIS controller of the UPQC for effectively resolving PQ issues [17].

Nevertheless, the ideal configuration of the novel-shaped fin was also found by simultaneously using CFD simulation and multi-objective response Surface Method optimization. The fin was then connected to a heat pipe and submerged in the LHTESS [18]. However, a comprehensive study utilizing passive cooling methods was collected and contrasted. The study also provided insight into selecting a cooling method suitable for a specific location or environmental factors [19]. Next, the sodium sulfated acetate with varying masses as a PCM comes next. By replacing the flexible blades under the panel with rigid blades and heated sinks, thermal conductivity was increased [20]. In the meantime, a thorough analysis of the literature on various swirl flow devices, rough surfaces, and turbulators for improving heat transfer in heat exchangers was attempted [21].

Subsequently, numerical modeling was carried out using a solar collector at the household scale. The curved physical boundaries were treated especially using the lattice Boltzmann method [22]. A strong fault-tolerant super-twisting sliding mode control technique was used to assess a two-stage, three-phase grid-connected photovoltaic inverter system under grid fault situations [23]. In addition, an expert knowledge-based proportional resonant control was proposed for connecting solar energy to the grid during abnormal grid circumstances to overcome the previously mentioned issue [24]. Furthermore, an efficient MPPT method was created using a hyperbolic slime mold algorithm. The optimizer framework equations utilize the hyperbolic tangent function to reduce significant perturbations during the tracking stage and enhance the convergence trend [25].

For precise RUL prediction, an enhanced anti-noise adjustable short-term long-term memory artificial neural network featuring high-robustness extraction of features and ideal parameter specifications has been suggested [26]. A more sophisticated feedforward-long term and short-term memory (FF-LSTM) modeling technique was presented, which takes into account changes in temperature, voltage, and current to achieve a precise whole-life-cycle SOC forecast. In order to create a new three-dimensional vector that will serve as the matrix of inputs for the filtering voltage and current, an optimal sliding balance window is built for the current being measured and filtering [27]. The FOPIDC and AI based hybrid controllers were selected for the wind system connected UPQC device to solve the PQ issues under different loading conditions [28,29].

Table 1 clearly shows that the majority of current research focuses on conventional methods like SRF and pq theories, often overlooking AI-based signal generation. Additionally, the optimal selection of filter parameters and controller gains has been largely neglected. Furthermore, although some studies considered design parameters, they did not take into account reduced switch-based multilevel converters to minimize losses.

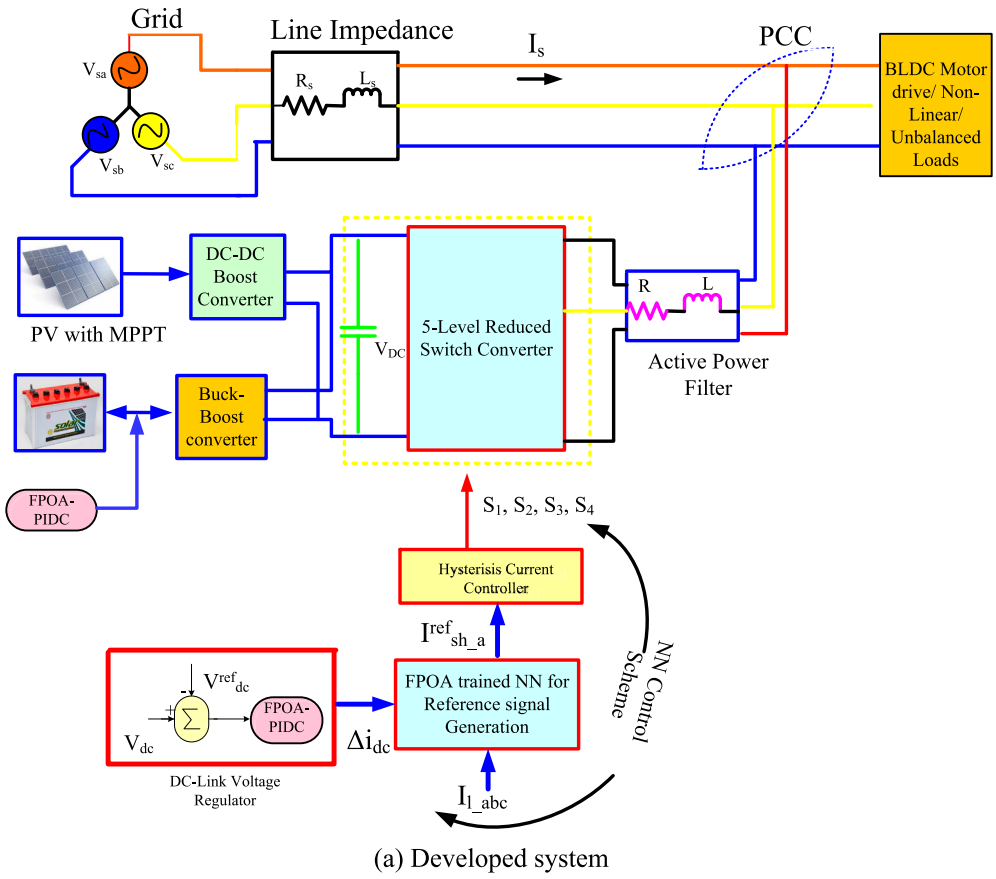

(a) Developed system

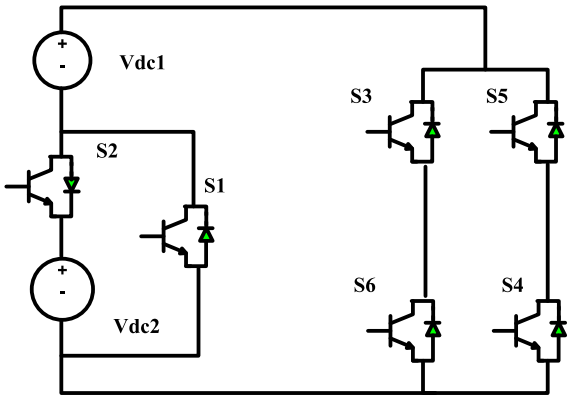

(b) Single phase reduced switch 5L-VSC

Fig. 1. Proposed reduced switch 5level converter configuration.

1.3. Novelty and contribution of the research work

- ➢ Implementation of a 5-level reduced-switch VSC for SHAPF to minimize switching losses.
- ➢ Development of PV in association with the energy storage battery integrated SHAPF by optimal selection of filter parameters like R, L along with the proportional integral derivative controller (PIDC) gain values for SHAPF and ESS controller with Flower Pollination Optimization Algorithm (FPOA).
- ➢ Selection of FPOA for optimal choice of weights and bias of NN for reference signal generation to avoid SRF and pq complex shifting.
- ➢ Prime objectives are to improve PF, attain a steady DC bus capacitor voltage (DCBCV) in a shorter period, and decrease the THD of the source current with power management to satisfy the load demand.
- ➢ Testing on three distinct scenarios, each characterized by varying loads and intensity of sun irradiation.

The paper's structure is as follows: Section 2 discusses the 5-level reduced switch VSC, with a specific emphasis on its external sources. Section 3 provides a detailed explanation of the control system that is recommended and utilizes FPOA. Section 4 presents the results and analysis. Finally, conclusion and future work in presented in Section 5.

2. Modeling of proposed system

Fig. 1(a) shows the schematic diagram of SHAPF tie up to the DC bus, coupled with the ideally integrated Solar Energy System (SES) and Energy Storage System (ESS). The reduced switch five-level VSC is linked

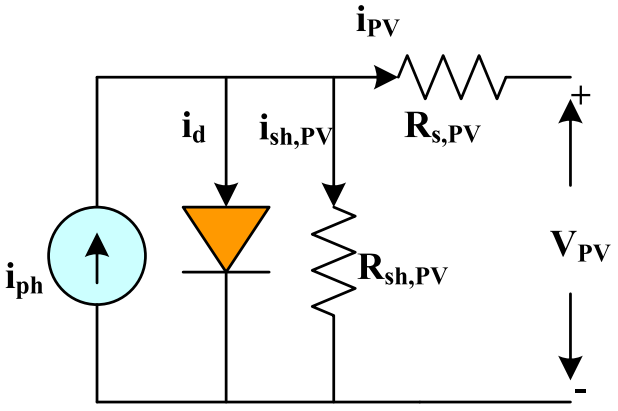

Fig. 2. PV single cell model.

in parallel to the load compensates harmonics, while also maintaining DCBCV. The cascaded H-Bridge inverter topology requires a larger number of switches to create a five-level output. The PWM circuit necessitates the use of eight switches to generate switching pulses. V_{dc1} and V_{dc2} represent the two capacitor voltages that are connected in the DC link.

This analysis proposes a modified switched topology of VSC in the context of a SHAPF combined with an optimized NN control technique.

Table 2
DC link power management.

Operational Modes	Action taken
1: *SES* is NIL	Only ESS will supply power to P_L.
2: $SES = P_L$	PV will handle P_L.
3: $SES < P_L$	The ESS will manage the difference power until $SOCB_{min}$.
4: $SES > P_L$	The PV is adopted to charge storage system until $SOCB_{max}$

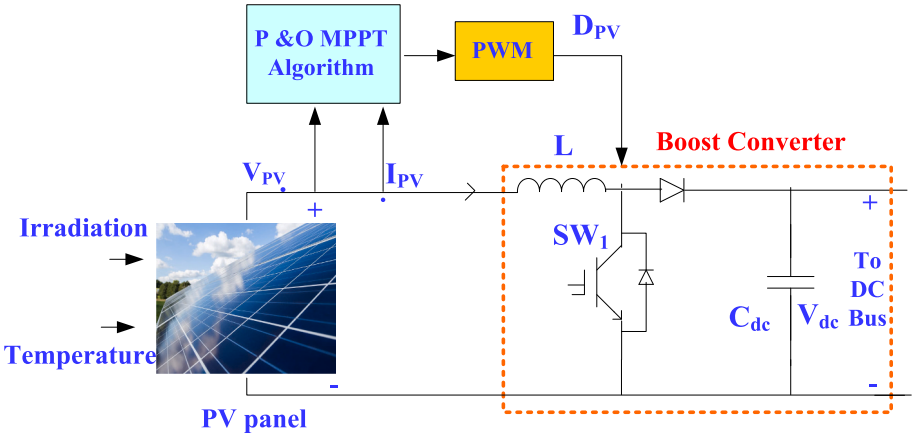

Fig. 3. Control of PV system.

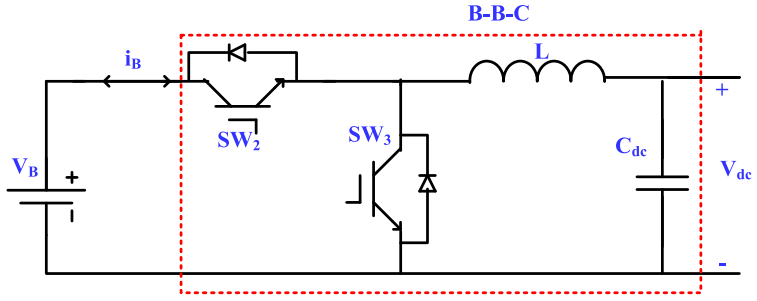

(a) ESS configuration at DC link

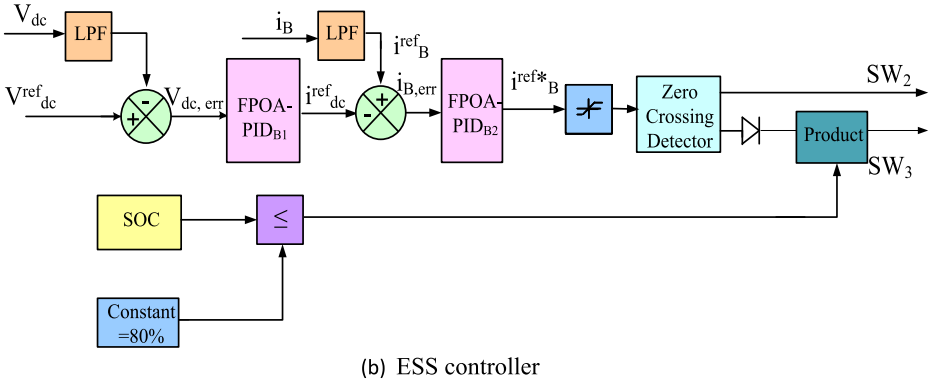

(b) ESS controller

Fig. 4. ESS with FPOA.

Table 3
PV and storage battery specifications.

Device	Parameters	Value
PV single panel (Sun power SPR-305E-WHT-D)	Series, parallel connected PV cells	5,11
	P_{max}	305.22 W
	I/ V at P_{max}	5.58 A/54.7 V
	Voltage and current under open and short circuit conditions	64.2 V/ 5.96 A
Li ion battery	Max voltage under charging	350 V
	Battery Capacity	35 Ah

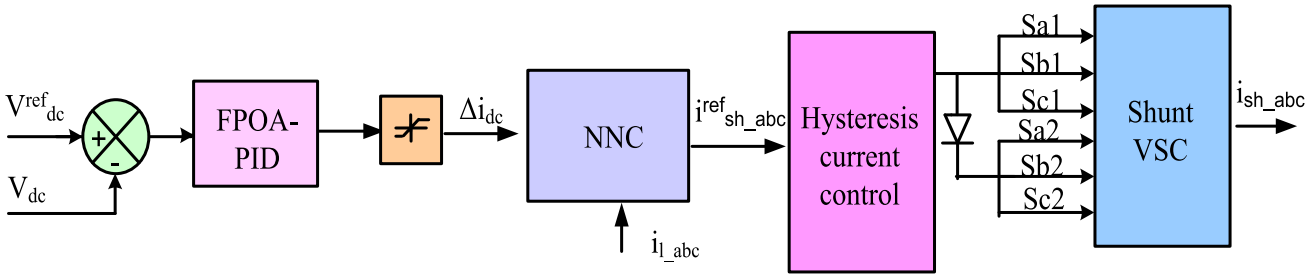

Fig. 5. Hybrid controller for shunt converter.

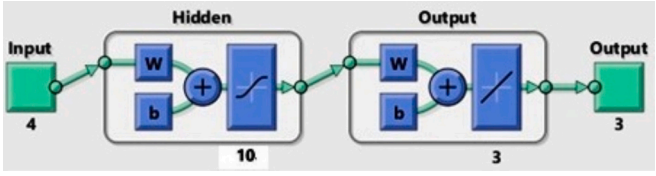

Fig. 6. Structure of NNC for reference current generation.

The modified diminished switch technique consists of two switches for level selection and a standard H-Bridge for polarity selection. Fig. 1(b) illustrates the suggested single-phase reduced switch multilevel inverter. In Fig. 1(b), switches S1 and S2 select the source/level, while the remaining switches are used for polarity selection. The operational rationale of the suggested inverter for achieving a 5-level output is as follows:

- SW_1, SW_3, and SW_4 are activated to achieve a positive voltage of V_{dc1}.
- SW_2, SW_3, and SW_4 are activated to obtain the + (sum of V_{dc1} and V_{dc2}).

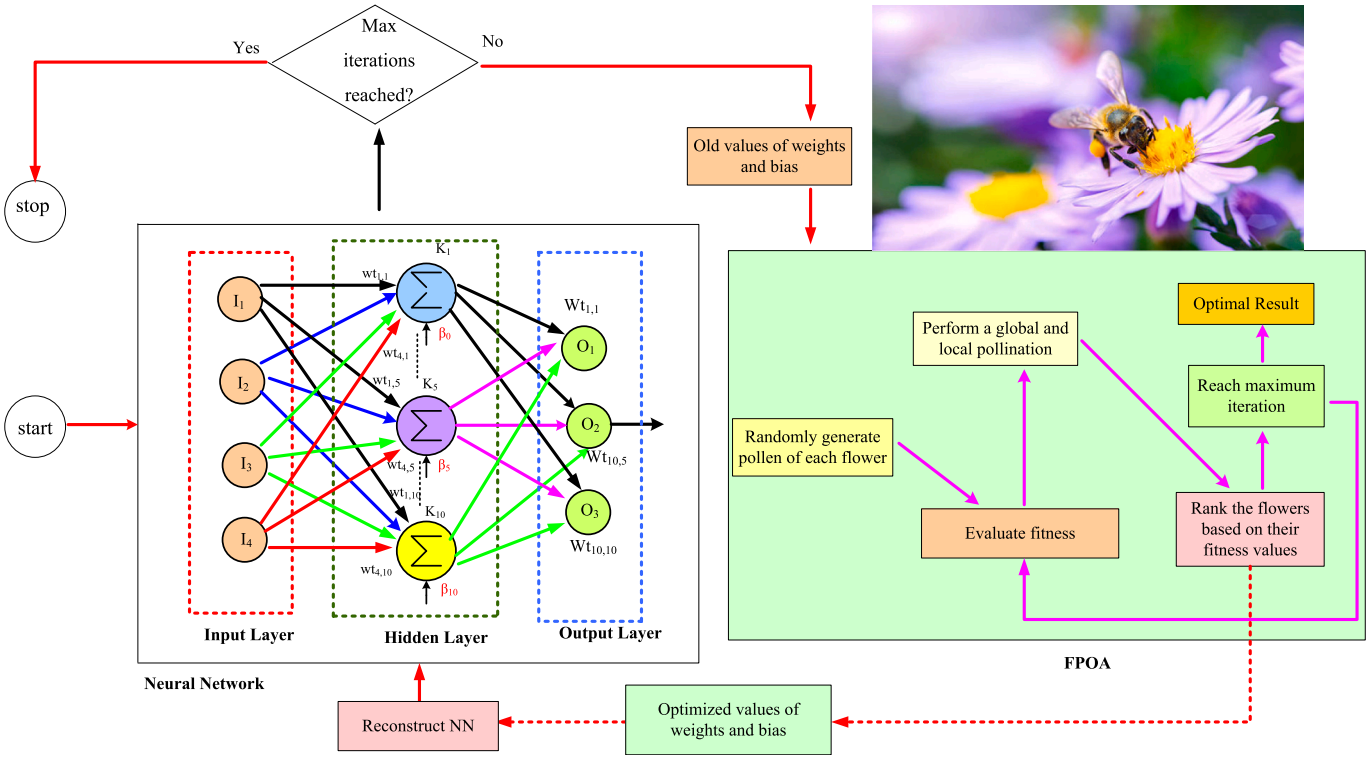

Fig. 7. FFOA trained NNC.

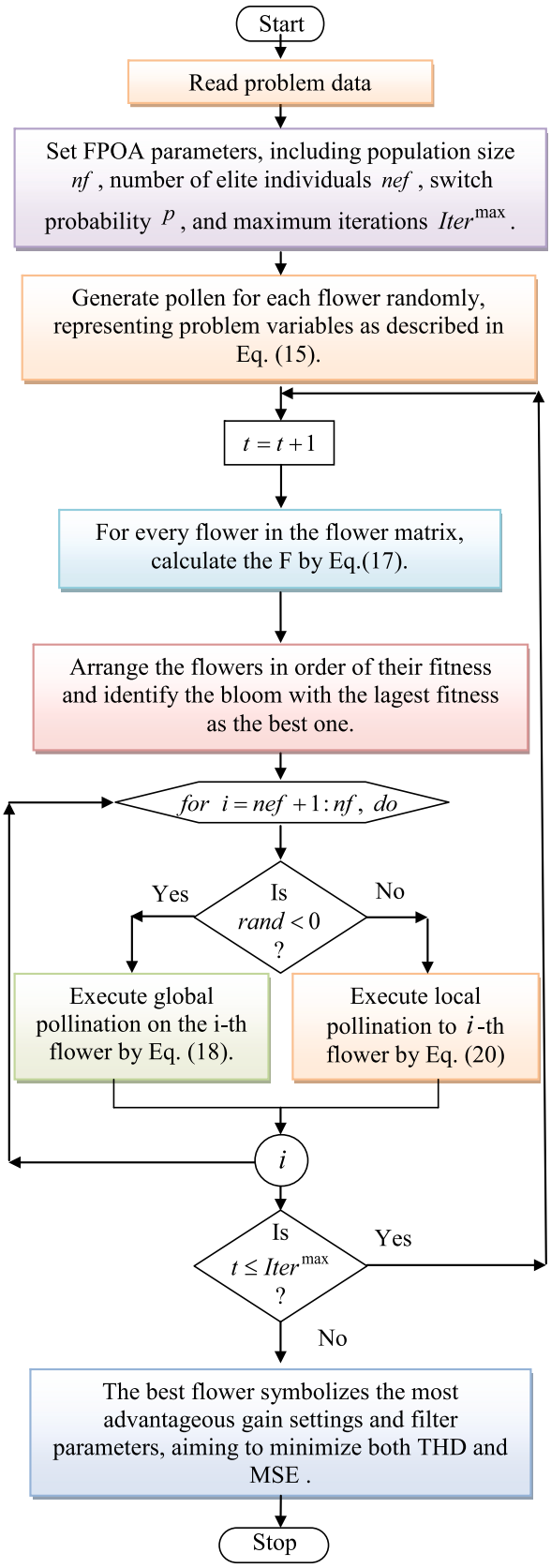

Fig. 8. Flow of the proposed FDGPS.

Table 4
System parameters.

Source	V_s: 415 V; R_s: 0.1 Ω; L_s: 0.15 mH; f: 50 Hz
DC bus	C_{dc}: 9400 microμF; $V^{ref}{}_{dc}$= 700 V

Table 5
Cases studies.

Load/condition	Case-1	Case-2	Case-3
Constant irradiation (1000 W/m^2)	✓		
Changeable irradiation		✓	✓
Load1: nonlinear balanced bridged rectifier: 60 Ω, 50 mH	✓	✓	✓
Load2: RL Unbalanced Load R1 = 10 Ω, R2 = 80 Ω, R3 = 130 Ω L1 = 9 mH, L2 = 15 mH, L3 = 28 mH			✓
Load3: BLDC drive	✓	✓	✓
Load4: Active reactive power load P = 1000 W, Q = 2000 var		✓	✓
Load5: Asynchronous motor load R = 500 Ω, L = 1 mH		✓	✓

Table 6
Total harmonic distortion (in %).

Ref []/Controller	Case1	Case2	Case3
Without SHAPF	29.47	14.09	24.17
SRF based PIC	4.336	3.987	4.235
pq based PIC	3.001	3.114	3.99
[2] ANFIS	3.73	–	–
[3] FLC-SMC	3.47	–	–
[5] PIC	4.01	–	–
[9] PIC	3.62	–	–
[12] ANN	3.52	–	–
FPOA-PIDC	3.32	2.93	3.98

- SW_1, SW_5, and SW_6 are activated to obtain a negative direct current voltage, denoted as $-V_{dc1}$.
- SW_2, SW_5, and SW_6 are activated to measure the – (sum of V_{dc1} and V_{dc2}).

Based on Fig. 1, it can be observed that the proposed configuration reduces the number of switches required for a five-level output. As a result, the three-phase recommended MLI reduces the number of switches by six. A reduction in the number of switches not only decreases the size but also the cost of the switching circuit. To achieve enhanced PQ, this topology suggests using a neural network-based reference signal generation approach instead of the traditional SRF and pq approaches.

2.1. SHAPF

The main purpose of SHAPF is to inject the required current at the PCC to ensure a distortion-free supply current. The controller circuit employs Eq. (1) to evaluate the precise amount of compensating current needed [13].

$$i_s = i_l - i_{sh} \tag{1}$$

$$V_s = V_m sinwt \tag{2}$$

$$i_l = \sum_{n=1}^{\infty} i_n sin(nwt + \varphi_n) \tag{3}$$

$$P_l = V_s^* i_l \tag{4}$$

Where, i_s, i_l, i_{sh} represents the source, load and compensating currents, V_s give supply voltage and P_l denotes load power. The numerical

value of C_{dc} can be obtained by [13] applying Eq. (5):

$$C_{dc} = \frac{\pi^{*} i_{sh}}{\sqrt{3}\omega V_{cr,pp}} \tag{5}$$

The available ratings supplied by the suggested approach are used to make the selection of$V^{ref}{}_{dc}$. Here, Peak-to-peak ripple voltage denotes $V_{cr,pp}$. The shunt side VSC is connected to the system via an inductor (L_{sh}), and its functions are dictated by the DCBCV, ripple current and switching frequency in the following ways [13]:

$$L_{sh,min} = \frac{\sqrt{3}\ m\ V_{dc}}{12\ a_f\ f_{sh}\ I_{cr,pp}} \tag{6}$$

With the premise that the peak-to-peak ripple current ($I_{cr,pp}$), over loading factor (a_f) of 1.5 switching frequency (f_{sh}) of 10 kHz, and modulating depth (m) is 1 define the value of (L_{sh}).

2.2. Mathematical modeling

The reduced number of switch configuration for VSC is recom-

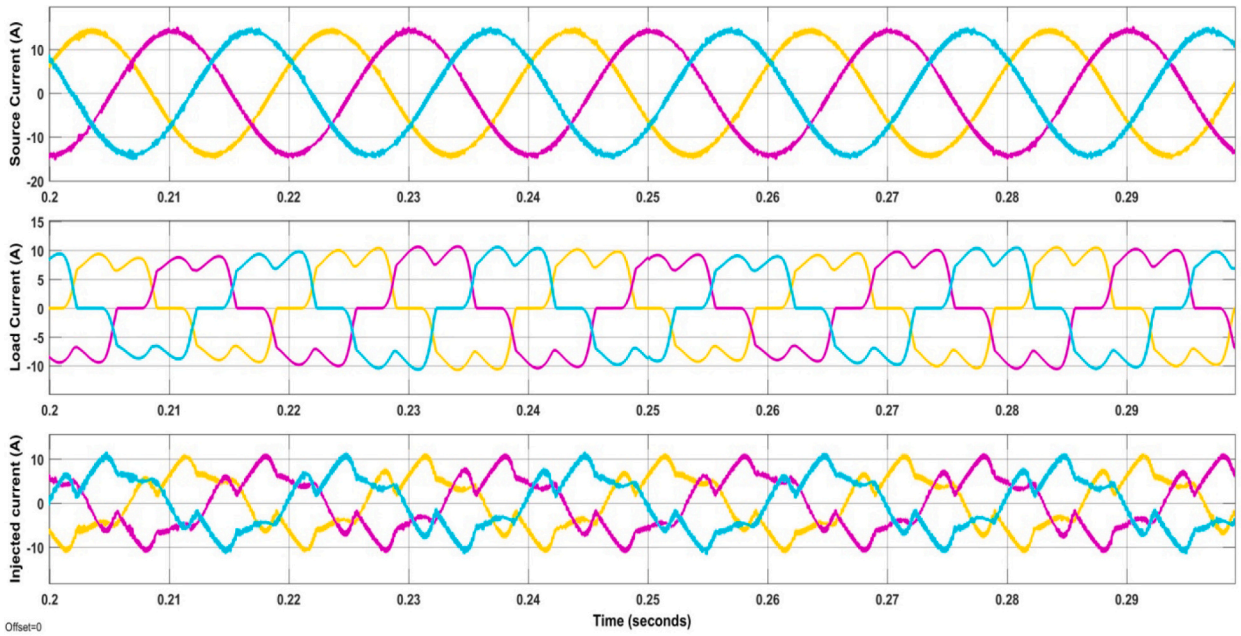

(a) i_l, i_{sh}, i_s

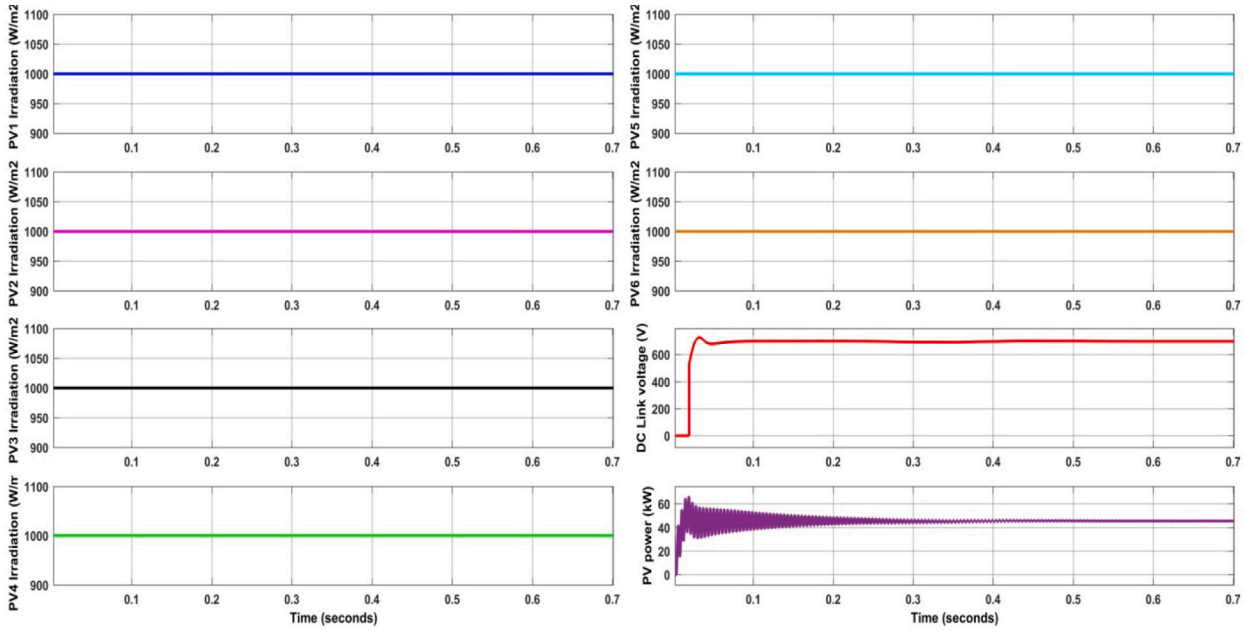

(b) Irradiation of six PV panels, P_L, DC bus voltage

Fig. 9. Waveforms for case1.

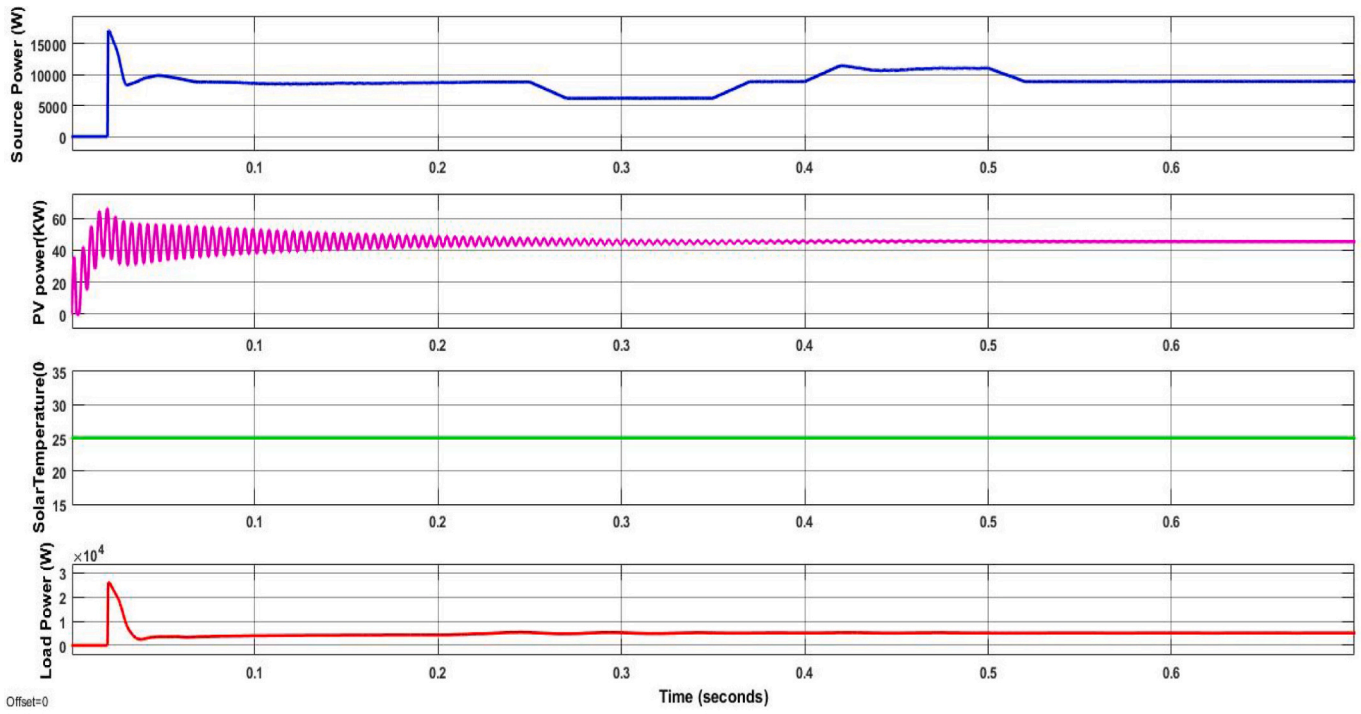

(c) Source power, PV power, T, Load power

Fig. 9. (*continued*).

mended in association with the solar and energy storage system is to supply power to the DC bus. The DCBCV is governed by PV, aided by ESS to manage variations in load side demand. Integration of these sources helps in decreeing the ratings and stress on converters. Eq. (7) gives power balance for the suggested method.

$$P_{PV} + P_G \pm P_{BSS} = P_L \tag{7}$$

2.2.1. SES

The Simulink library model PV was utilized in this work. Here, PV modules are joined in series to get a string to achieve the essential current and voltage. Each cell in the module is built with a more basic circuit that consists of only one diode, as shown in Fig. 2.

Eq. (8) [13] applies KCL to calculate the output current of the PV cell.

$$i_{PV} = i_{ph} - i_d - i_{sh,PV} \tag{8}$$

Eq. (9) is employed to establish the connection of PV modules in both parallel and series configurations, resulting in the formation of an array.

$$i_{PV,m} = i_{ph}N_p - i_{S,PV}N_p\left[exp\left(\frac{Q\left(V_{PV} + N_s/N_p\left(i_{PV,m}R_{S,PV}\right)\right)}{N_s\eta kT_C}\right) - 1\right] - \frac{V_{PV,m} + N_s/N_p\left(i_{PV,m}R_{S,PV}\right)}{N_s/N_p\left(R_{sh,PV}\right)} \tag{9}$$

Here,

$$i_{ph} = \left(i_{ph,n} + K_1\Delta T_C\right)\frac{G}{G_n} \tag{10}$$

Where, V_{PV}, P_{PV}, i_{PV} gives voltage, power and current of solar system. i_d, i_{ph}, $i_{sh,PV}$ are diode, photo current, and shunt current of PV. T indicates solar temperature, N_s number of cells in series, N_p number of cells in parallel, and G solar irradiation.

Eq. (11) describes the output of PV, which is controlled by the system shown in Fig. 3. In this study, the P & O based MPPT approach was utilized to derive the maximum output.

$$P_{PV} = V_{PV} \times i_{PV} \tag{11}$$

2.2.2. ESS

Strengths of the ESS include less discharge and less maintenance requirements. As seen in Fig. 4(a), switches SW1 and SW2 can be used to charge or drain the battery. The state-of-charge for the battery considered (*SOCB*) [13] indicated by Eq. (12):

$$SOCB = 80\left(1 + \int i_{BS}\ dtQ\right) \tag{12}$$

The charging or discharging capacity of the battery depends on the amount of P_{PV} and *SOC* boundaries.

$$SOCB_{\min} \le SOCB \le SOCB_{\max} \tag{13}$$

The terms "$SOCB_{max}$" and "$SOCB_{min}$" represent the upper and lower limits for the allowable SOCB of the battery. Fig. 4 (b) illustrates the control circuit that is responsible for regulating the battery operation.

The reference current ${i^{ref}}_{dc}$ is estimated by minimizing the DC-bus voltage error with a PID controller selected through FPOA. The reference current error for the battery $i_{B,err}{}^*$ is determined by optimizing the PID controller for battery current error. Here $i_{B,err}$ represents the variance between ${i^{ref}}_{dc}$ and ${i^{ref}}_B$.

Table 2 illustrates the coordination of power management among the SES, ESS, electrical grid, and energy demand, and Table 3 showcases the selected values for SES and ESS.

3. Control technique

The prime goals of SHAF are to ensure the stability of DCBCV and reduce waveform irregularities by delivering an appropriate current. The proposed control scheme provides (i) FPOA-trained NNC for reference signal generation and (ii) a tuned PIDC system developed for SHAPF and ESS and the optimal choice of filter variables to fulfill the

specific objectives. This work aims to emphasize the control method of the proposed FPOA-tuned PIDC and FPOA-trained NNC.

3.1. FPOA optimized PIDC and NN based reference signal generation

The SHAPF's effectiveness relies on generating the reference current and regulating the DCBCV. However, fluctuations in load can lead to changes in power flow, affecting the stability of the DCBCV. To maintain stability, the SHAPF must address switching losses. The FPOA-based gain values selected for the PIDC introduces an error, which is quantified by computing the disparity between the set and true DCBCV by Eq. (14), as shown in Fig. 5.

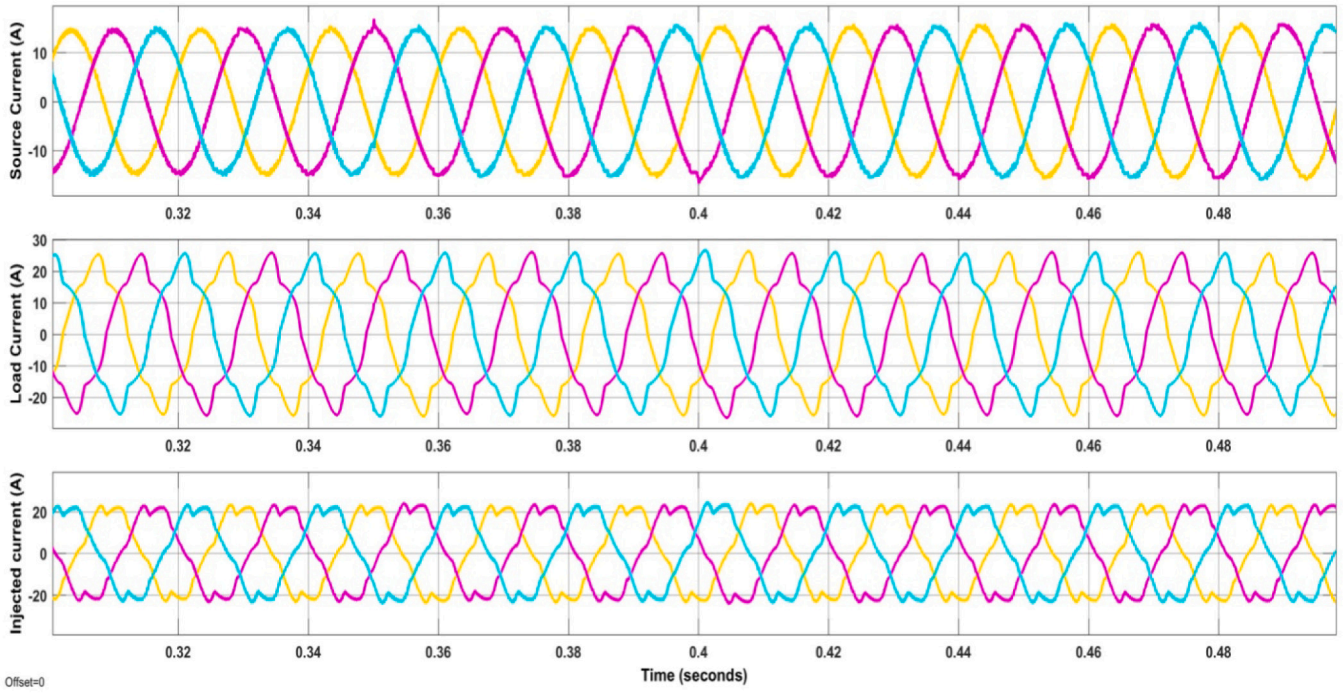

(a) i_l, i_{sh}, i_s

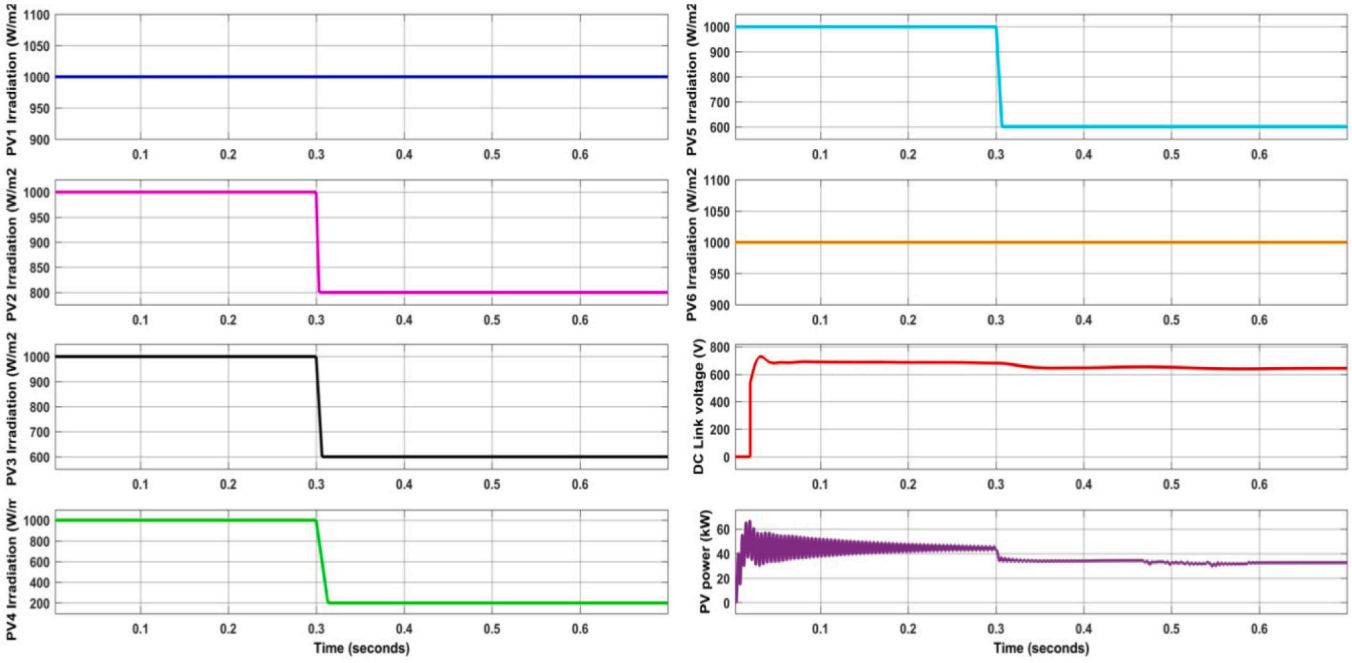

(b) Irradiation of six PV panels, P_L, DC bus voltage

Fig. 10. Waveforms for case2.

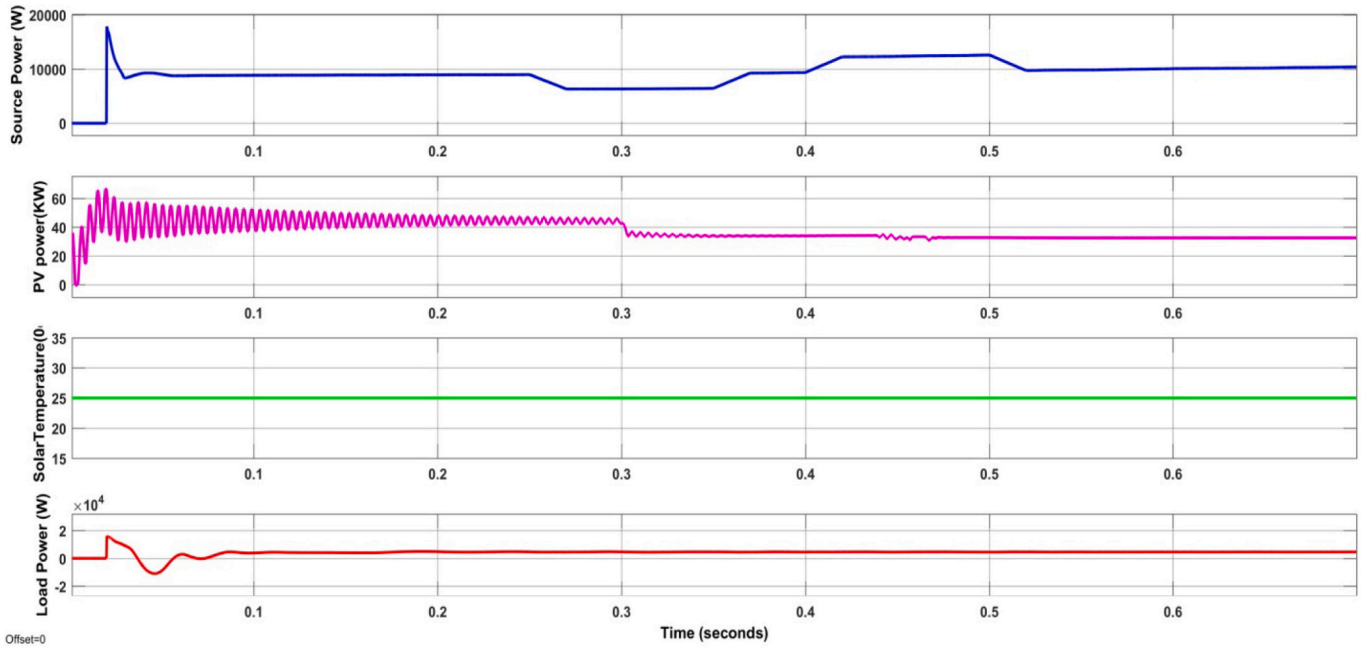

(c) Source power, PV power, T, Load power

Fig. 10. (*continued*).

$$\Delta i_{dc} = e_1(t) = V^{ref}{}_{dc} - V_{dc}(t) \tag{14}$$

FPOA trained NNC based reference signal generation is adopted to avoid complex SRF and pq transformations. The shunt reference currents $i^{ref}_{sh\_abc}$ i.e. ($i^{ref}_{sh\_a}$, $i^{ref}_{sh\_b}$,$i^{ref}_{sh\_c}$) are regarded as target data, whereas the load currents i_{L_abc} i.e. (i_{L_a}, i_{L_b},i_{L_c}) and Δi_{dc} acquired from FPOA optimized PIDC are considered as input. Here, NNC is trained by adopting FPOA.

Fig. 6 depicts the structure of NNC and Fig. 7 depicts the FPOA trained NNC.

Flowering plants, which are the predominant species in the environment, have undergone evolutionary changes through the process of flower pollination for about 125 million years. The primary function of a flower is to facilitate reproduction through the process of pollination, which involves the transfer of pollen by various pollinators such as birds and other insects. Two methods of pollination exist: abiotic and biotic. In biotic pollination, the transfer of pollen occurs through the assistance of a pollinator, such as an animal or insect. On the other hand, abiotic pollination does not include any pollinators. 90 % are biotic pollination, while remaining undergo abiotic.

Both self-pollination and cross-pollination are possible methods of pollination. The movement of pollen from one flower of a different plant to another is referred to as cross-pollination. On the other hand, self-pollination occurs when a flower is fertilized by pollen from the same flower or from other flowers of the same plant. This typically happens when there is no dependable pollinator present. Due to the extensive flight capabilities of pollinators such as birds and bees, cross-pollination can occur across significant distances. This type can be called global pollination. In addition, birds and bees may exhibit levy flight behavior, where their flying or jumping distances follow a Levy distribution. The process of flower pollination, which aims to efficiently reproduce plants, may be represented as an optimization process. This can be achieved by following four steps in constructing FPOA:

Step 1: Global pollination is facilitated by cross and biotic-pollination processes, with pollinators exhibiting Levy flight patterns.

Step 2: Self-pollination and abiotic that occurs within a specific area and do not rely on any external support.

Step 3: Flower constancy, which is a behavior shown by insects, is comparable to a measure of the likelihood of reproduction, indicating the degree of similarity between two blooms.

Step 4: The interaction between global and local pollination is controlled by a switch probability that is slightly skewed towards local pollination.

While it is possible for each plant to have several blooms, for the sake of simplicity, every plant is said to have a single flower that produces a single pollen gamete. Each bloom and/or pollen gamete in this algorithm serves as a solution point for the problem. In this work, the problem variables are the filter parameters along with battery and shunt filter PIDC gain values in addition to weights and bias of NN. Each flower in FPOA is therefore represented in vector form to denote the problem variables as

$$\beta = \begin{bmatrix} K_p, K_i, K_D, K_{pB1}, K_{iB1}, K_{DB1}, K_{pB2}, K_{iB2}, K_{DB1}, \\ wt_{1,1}\ldots wt_{1,5}, \ldots wt_{1,10}, \ldots wt_{2,1}, \ldots\ldots wt_{3,1}, \ldots, wt_{4,1}\ldots\ldots \\ Wt_{1,1}, \ldots Wt_{5,1}, \ldots Wt_{10,1}\ldots\ldots, \beta_0, \ldots \beta_5, \ldots \beta_{10}, R, L \end{bmatrix} \tag{15}$$

The limits are shown as

$$\beta_{i(min)} \le \beta_i \le \beta_{i(max)}; i = 1, 2\ldots n \tag{16}$$

The fitness (F) can be constructed using the restrictions and the normalized objective functions, which assign equal importance to all selected objectives while accommodating both minimization and maximization functions.

$$\begin{aligned} Maximize F &= \frac{1}{1 + (obj_1, obj_2)} \\ obj_1 &= MSE = \frac{1}{n}\sum_{p=1}^{m} (O - \overline{O})^2 \\ obj_2 &= THD = \frac{\sqrt{(I^2{}_2 + I^2{}_3 + \ldots . I^2{}_n)}}{I_1} \end{aligned} \tag{17}$$

Here, $\overline{o}$ is the desired result, $o$is the output that was obtained, and m is the number of instances. The fundamental and harmonic components of current are resembles by I_n, I_1. The optimization approach for minimizing the cost function of Eq. (18) considers both global and local pollinations. During global pollination, insects facilitate the movement of pollen gametes across vast distances, so enabling the pollination and reproduction of the most genetically superior organisms. This crucial stage in global pollination can be symbolized by:

$$\beta_l^{t+1} = \beta_l^t + \gamma\ L(\lambda)\ \left(\beta_l^t - g^*\right) \tag{18}$$

Where, β_l^t is the location of the flower's pollen at the -th iteration, and g^* is the current best answer discovered among all solutions at the t^{th} generation. A γscaling factor is present to regulate the size of the steps. Given that pollinators need to traverse extensive distances utilizing various step lengths, a Levy flight is employed to accurately represent this behavior. A Levy distribution with L>0 is defined as

$$L \approx \frac{\lambda\Gamma(\lambda)sin(\pi\lambda/2)}{\pi}\frac{1}{s^{1+\lambda}}, (s \gg s_0 >) \tag{19}$$

Let β_n^t and β_p^tdenote pollen gametes of the same plant.εresembles the random uniform distribution ranging from 0 to 1. In theory, flower pollination can happen at both local and global levels. Flowers are primarily pollinated by nearby flowers rather than those located at a distance. To simulate this process, one can utilize a switch probability$p \in [0,1]$ (Step 4) to alternate between local and global pollination in an efficient manner. Typically, a value of $p = 0.8$ yields superior outcomes for most applications.

The initial population of flowers is created by randomly generating

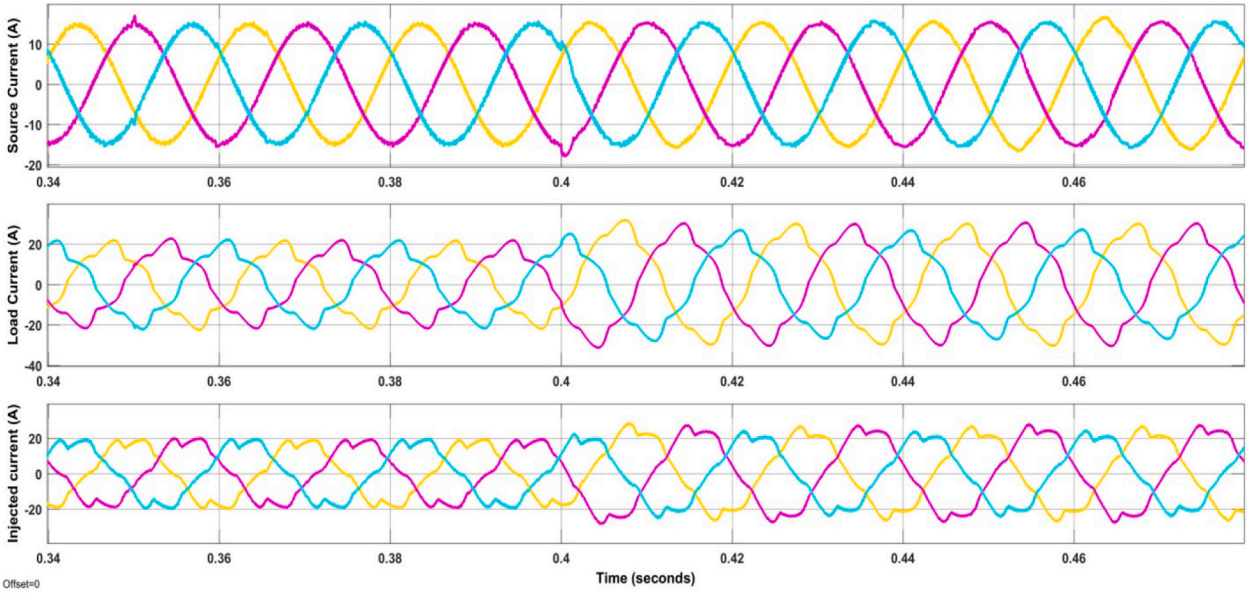

(a) i_l, i_{sh}, i_s

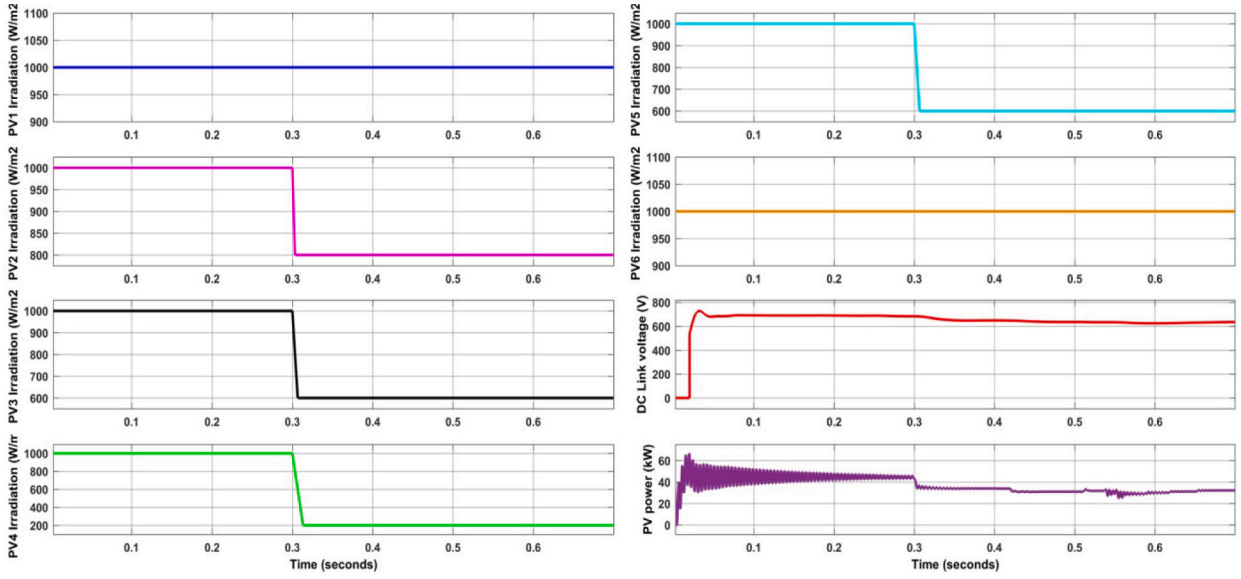

(b) Irradiation of six PV panels, P_L, DC bus voltage

Fig. 11. Waveforms of case3.

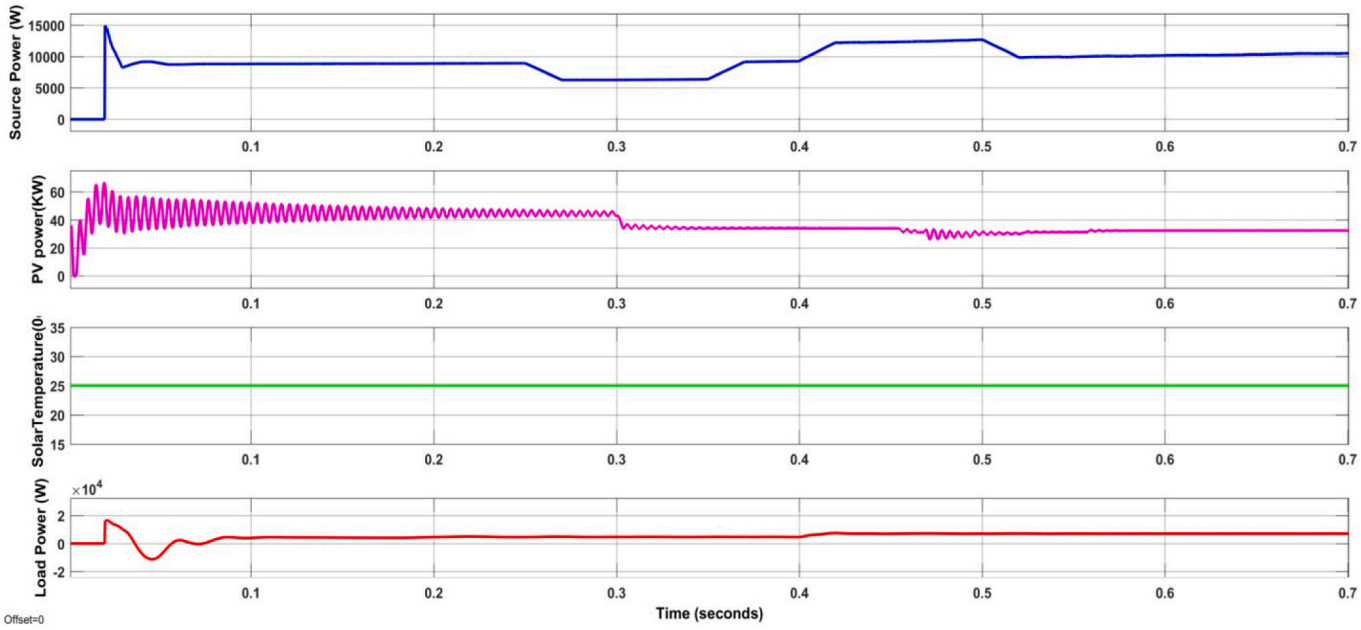

(c) Source power, PV power, T, Load power

Fig. 11. (*continued*).

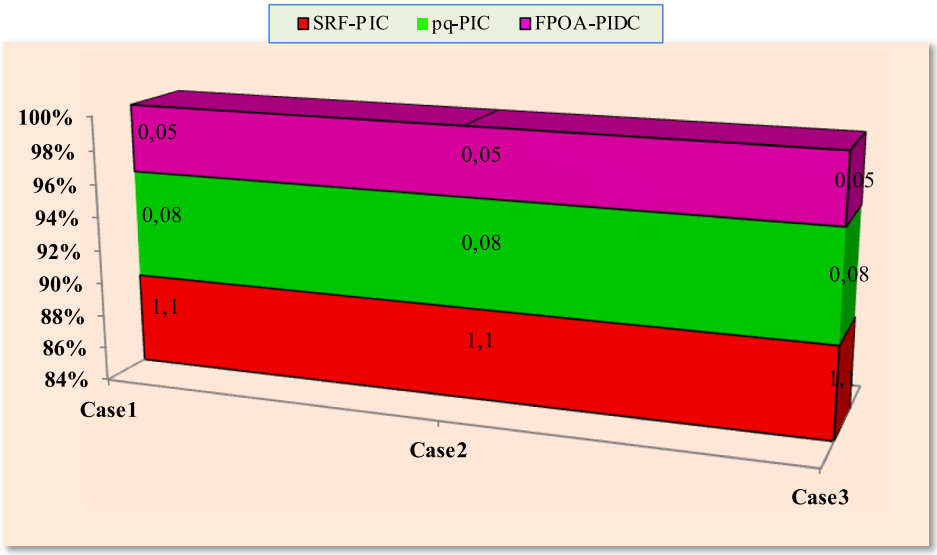

Fig. 12. Time (in seconds) to obtain steady DCBCV.

values within their respective bounds. The F is evaluated using the parameters specified in every flower. The local, gobal pollination procedure is then applied to all the flowers in the population to maximize their fitness. The iterative approach is continued till the convergence is obtained. Fig. 8 illustrates the sequence of actions in the proposed FPOA. The symbol "$\Gamma(\lambda)$" denotes a gamma. The distribution mentioned above is applicable for significant increments $s>0$. Step 2 and Step 3, which depict the process of local pollination, can be represented, or simulated as

$$\beta_l^{t+1} = \beta_l^t + \varepsilon\left(\beta_n^t - \beta_p^t\right) \tag{20}$$

Like other metaheuristic algorithms, the success of FPOA often depends on how well it is configured and tailored to a particular problem domain. It is highly efficient with exponential convergence rate based on the comparison of other algorithms and applicable for solving multi-objective optimization problems though it has its own drawbacks like inadequate optimization precision.

4. Simulation and results

The provided method was evaluated by conducting experiments on a 3-φ local network. To assess the efficacy of the proposed approach, three distinct test scenarios were selected. These scenarios included different combinations of loads, like 3Θ bridged RL rectifier, imbalance RL branch, an asynchronous motor, and a BLDC motor drive loads with different conditions of SES. Table 4 contains the specific information about the system parameters. Besides, Table 5 gives the test studies

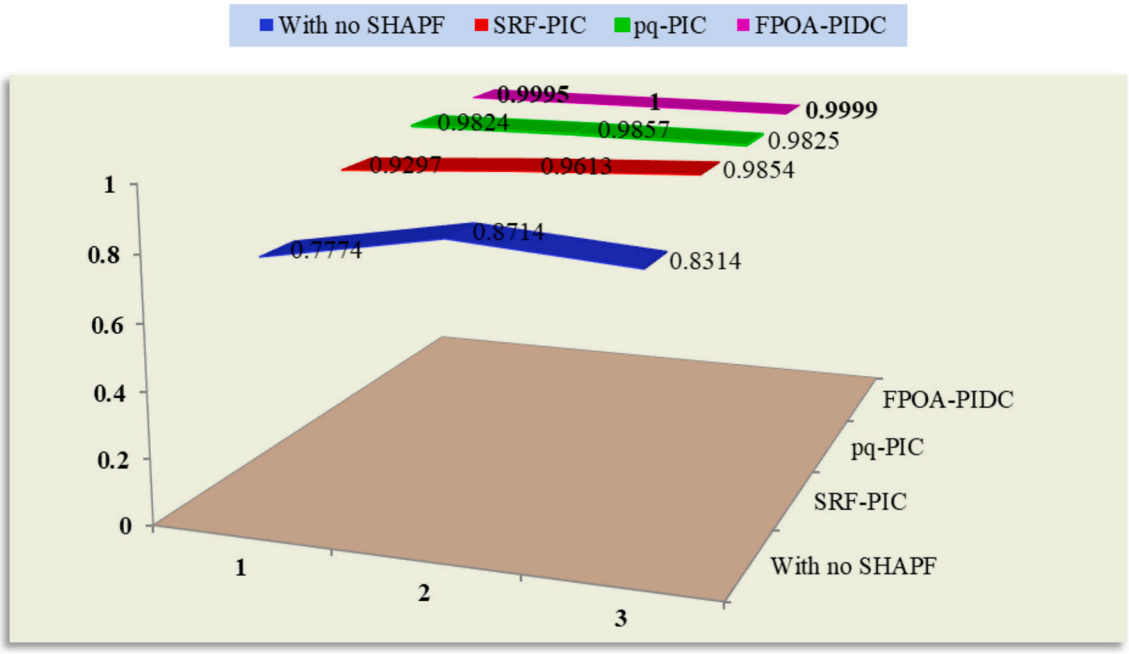

Fig. 13. Power Factor Comparison.

considered in the research work.. Besides, the THD of the developed technique was evaluated and compared against the standard employed SRF and pq approaches with PIC in Tables 6 for each test scenario.

Table 5 shows that in test case 1, the current at the load is not sinusoidal and distorted when Load 1 and Load 3 are linked. With a THD of 29.47 % and a PF of 0.7774, it is balanced, nevertheless. The output waveforms for case studies 1–3 are illustrated Figs. 9–11. These provides the supply/grid as V_s, load voltage represents V_l, DCBCV as V_{dc}, load current resembles i_l, filter injection currents gives i_{sh}, and supply current denotes i_s, irradiation as G, temperature as T.

The developed technique delivers a supply current free of harmonics, as shown in Fig. 9(a). As shown in Table 6, there was a noticeable drop in the THD in addition to the current waveforms. The THD of the load current decreased from 29.47 % to 3.32 % and the PF increased from 0.7774 to 0.9995 by adding the appropriate shunt currents—a lower value compared to other traditional ways and recorded approaches. Six PV panels were taken into consideration, as shown in Fig. 9(b), but with set temperatures and irradiance as well as maximum PV output power. However, under set G and T conditions, the suggested approach successfully produced a steady DC bus voltage in less than 0.05 s. In addition, Fig. 9(c) shows how the source, PV, and load may effectively manage power under conditions of constant temperature.

As illustrated in Fig. 10(a), the current at load in case 2 is enormously polluted and distorted due to the integration of Loads 1, 3, 4 and 5 simultaneously. The PF is measured to be 0.8714, while the THD is found to be 14.09 % in the absence of a filter. Fig. 10(a) illustrates the capability of the developed method to supply harmonics free current by removing imperfections in waveforms through injecting the compensating current. The PF has been raised to 1, resulting in a drop in the THD of the load current from 14.09 % to 2.93 %. Besides, it can be seen from Fig. 10(b) that variable irradiation were considered for different PV panels it is clear that the FPOA tuned PIDC rapidly settles the DC bus voltage at a consistent level, even during fluctuations in *G*. On other hand, power management was handled effectively to maintain consistent power to the load.

In addition, case-3 illustrates a comparable pattern of decreasing the harmonics and raising the PF. The current signal of load exhibits a non-sinusoidal waveform until 0.4 s due to the presence of load 1, 3, and 5. Subsequently, at 0.4 s, load 2 and 4 were interconnected, resulting in a non-sinusoidal waveform with unbalanced characteristics and an amplified current magnitude due to flaws. Fig. 11 (a) illustrates that the proposed method effectively addresses the limitations in the current waveform. In addition, Fig. 11 (b) illustrates that the suggested method successfully preserves the stability of the DC bus voltage under varying irradiation conditions. Finally, it offers exceptional performance in power management.

This study entails doing FFT analysis on all 3 test studies. Specifically, this component examines the outcomes of test case 3, which included the utilization of several loads in combination with a BLDC drive and an asynchronous motor. Fig. 12 exhibits the documented duration needed to attain stable DC Bus voltage regulation across different control schemes. It is clear from that the FPOA tuned PIDC based SHAPF can generate a stable DC Bus voltage in less than 0.05 s.

The PF comparison for each situation is shown in Fig. 13.

In Fig. 14, the THD spectra for each case is shown.

The discussions mentioned above clearly illustrate that the suggested method with the association of flower pollination-based metaheuristic algorithms for the appropriate selection of reference signals for pulse generation, PIDC gain values, bias and weights of neural network and filter parameters is very efficient in decreasing THD, improving PF, with lower settling time period of DC bus voltage. However, the suggested method eliminates the need for complex transformations that are used in conventional SRF and pq theories.

5. Conclusion

This research introduces a five-level reduced-switch shunt VSC to decrease the number of switches required for the SHAPF. The FPOA is employed to optimally select the gain values of the PID controller for both the shunt filter and ESS controllers. Additionally, this algorithm is used for training the neural network-based reference signal generation, eliminating the need for conventional transformations. This approach enables quick regulation of the DCBCV, reduces THD, and improves PF with efficient power management.

The proposed controller effectively minimizes THDs to within allowable limits, achieving 3.32 %, 2.93 %, and 3.98 %, and boosts the PF to 0.9995, 1, and 0.9999 through proper power management. These results were observed across three test scenarios with different load

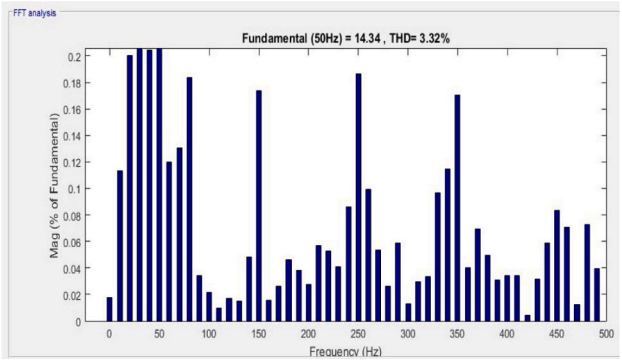

(a) Case-1

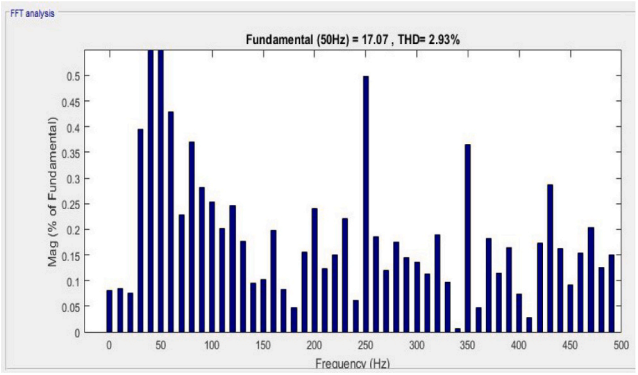

(b) Case-2

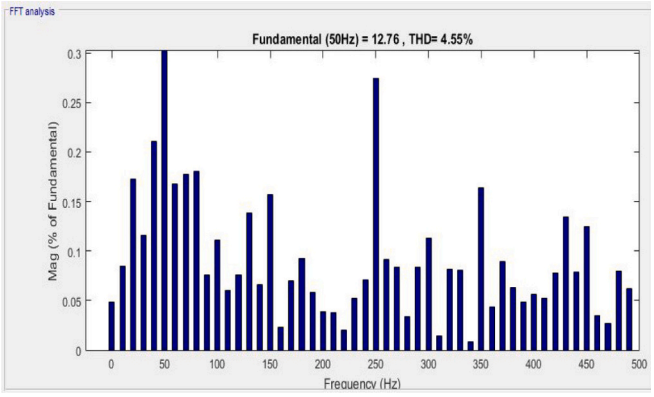

(c) Case-3

Fig. 14. FFT spectrum.

configurations and both fixed and variable G. The developed method outperforms standard techniques such as SRF and pq theories with PIC, as well as other methods available in the literature. Additionally, the proposed system achieves a stable DC bus voltage in just 0.05 s, compared to 0.08 and 1.1 s required by other methods.

In future research, the proposed model will be extended to work with reduced-switch 7-level converters. The focus will be on optimizing hybrid AI controllers, such as ANFIS, for hybrid power filters and parameter design. This will involve treating both the filter and controller design as an optimization problem, utilizing the latest metaheuristic algorithms.

CRediT authorship contribution statement

Koganti Srilakshmi: Writing – original draft, Investigation, Formal analysis, Conceptualization. **Amit Kumar:** Writing – review & editing, Visualization, Supervision, Resources, Project administration, Formal analysis, Conceptualization. **Krishnaveni Kondreddi:** Software, Investigation, Data curation, Conceptualization. **T. Murali Krishna:** Writing – original draft, Visualization, Investigation, Formal analysis. **Praveen Kumar Balachandran:** Resources, Methodology, Investigation, Conceptualization. **Gianluca Gatto:** Writing – review & editing, Validation, Resources, Investigation, Funding acquisition.

Declaration of competing interest

The authors declare that they have no known competing financial interests or personal relationships that could have appeared to influence the work reported in this paper.

Data availability

Data will be made available on request.

Acknowledgments

This study was partially funded by the projects “Network 4 Energy Sustainable Transition – NEST (PE0000021)” and e.INS – Ecosystem of Innovation for Next Generation Sardinia (ECS00000038)” under the National Recovery and Resilience Plan (NRRP) of the Italian Ministry of University and Research under the Next-Generation EU Program.

References

[1] S. Devassy, B. Singh, Performance analysis of solar PV array and battery-integrated unified power quality conditioner for microgrid systems, IEEE Trans. Ind. Electron. 5 (2020) 4027–4035, https://doi.org/10.1109/TIE.2020.2984439.
[2] Koganti Srilakshmi, et al., A renewable energy source fed neuro-fuzzy controlled multilevel UPQC for power quality improvement, Int. J. Renew. Energy Res. 14 (2) (June 2024).
[3] Koganti Srilakshmi, et al., Development of AI controller for solar /battery fed H-bridge cascaded multilevel converter UPQC under different loading conditions, Int. J. Renew. Energy Res. 14 (2) (2024).
[4] Koganti Srilakshmi, et al., Design and performance analysis of fuzzy based hybrid controller for grid connected solar-battery unified power quality conditioner, Int. J. Renew. Energy Res. 13 (1) (March 2023), https://doi.org/10.20508/ijrer.v13i1.13318.g8655.
[5] K. Srilakshmi, et al., Performance analysis of artificial intelligence controller for PV and battery connected UPQC, Int. J. Renew. Energy Res. 13 (1) (March 2023), https://doi.org/10.20508/ijrer.v13i1.13523.g8672.
[6] K. Srilakshmi, et al., Design and performance analysis of hybrid controller for self tuning filter based solar integrated UPQC, Int. J. Renew. Energy Res. 13 (1) (2023), https://doi.org/10.20508/ijrer.v13i1.13523.g8672.
[7] K. Srilakshmi, et al., Design of soccer league optimization based hybrid controller for solar-battery integrated UPQC, IEEE Access 10 (2022) 107116–107136, https://doi.org/10.1109/ACCESS.2022.3211504.
[8] Koganti Srilakshmi, Rao Gummadi Srinivasa, Balachandran Praveen Kumar, Senjyu Tomonobu, Green energy-sourced AI-controlled multilevel UPQC parameter selection using football game optimization, Front. Energy Res. 12 (2024), https://doi.org/10.3389/fenrg.2024.1325865.
[9] Muhammad AlifMansor, Kamrul Hasan, Muhammad Murtadha Othman, Construction and performance investigation of three-phase solar PV and battery energy storage system integrated UPQC, IEEE Access 8 (2020) 103511–103538, https://doi.org/10.1109/ACCESS.2020.2997056.
[10] N.C. Sai Sarita, S. Suresh Reddy, P. Sujatha, Control strategies for power quality enrichment in Distribution network using UPQC, in: Materials Today: Proceedings 80, 2023, pp. 2872–2882. Part 3.
[11] Koganti Srilakshmi, et al., Optimal design of solar/wind/battery and EV fed UPQC for power quality and power flow management using enhanced most valuable player algorithm, Front. Energy Res. 11 (2024), https://doi.org/10.3389/fenrg.2023.1342085.
[12] K. Chandrasekaran, J. Selvaraj, C.R. Amaladoss, L. Veerapan, Hybrid renewable energy based smart grid system for reactive power management and voltage profile enhancement using artificial neural network, Energy Sour. A 43 (19) (March 2021) 2419–2442.
[13] K. Srilakshmi, D.T. Santosh, A. Ramadevi, et al., Development of renewable energy fed three-level hybrid active filter for EV charging station load using Jaya grey wolf

optimization, Sci. Rep. 14 (2024) 4429, https://doi.org/10.1038/s41598-024-54550-7.
[14] A. Ramadevi, K. Srilakshmi, P.K. Balachandran, I. Colak, C. Dhanamjayulu, B. Khan, Optimal design and performance investigation of artificial neural network controller for solar- and battery-connected unified power quality conditioner, Int. J. Energy Res. 3355124 (2023) 22, https://doi.org/10.1155/2023/3355124.
[15] Koganti Srilakshmi, et al., Simulation of grid/standalone solar energy supplied reduced switch converter with optimal fuzzy logic controller using golden Ball Algorithm, Front. Energy Res. 12 (2024), https://doi.org/10.3389/fenrg.2024.1370412.
[16] Koganti Srilakshmi, et al., "Multiobjective Neuro-Fuzzy Controller Design and Selection of Filter Parameters of UPQC Using Predator Prey Firefly and Enhanced Harmony Search Optimization", International Transactions on Electrical Energy Systems, Volume, 2024, https://doi.org/10.1155/2024/6611240 (Article ID 6611240, 21 pages).
[17] K. Srilakshmi, G.S. Rao, K. Swarnasri, et al., Optimization of ANFIS controller for solar/battery sources fed UPQC using an hybrid algorithm, Electr. Eng. (2024), https://doi.org/10.1007/s00202-023-02185-8.
[18] Sina Lohrasbi, Seyed Ziaedin Miry, Mofid Gorji-Bandpy, Davood DomiriGanji, Performance enhancement of finned heat pipe assisted latent heat thermal energy storage system in the presence of nano-enhanced H2O as phase change material, Int. J. Hydrog. Energy 42 (10) (2017) 6526–6546, https://doi.org/10.1016/j.ijhydene.2017.01.045.
[19] Arash Mahdavi, Mousa Farhadi, Mofid Gorji-Bandpy, Amirhoushang Mahmoudi, A review of passive cooling of photovoltaic devices, Cleaner Eng. Technol. 11 (2022) 100579, https://doi.org/10.1016/j.clet.2022.100579.
[20] Ali Gholami, Mofid Gorji, Experimental study for the use of Na2SO4.10H2O as a PCM with fixed blades for temperature and efficiency parameters of photovoltaic panel, Case Stud. Therm. Eng. 49 (2023) 103219, https://doi.org/10.1016/j.csite.2023.103219.
[21] Mohsen Sheikholeslami, Mofid Gorji-Bandpy, Davood Domiri Ganji, Review of heat transfer enhancement methods: Focus on passive methods using swirl flow devices, Renew. Sust. Energ. Rev. 49 (2015) 444–469, https://doi.org/10.1016/j.rser.2015.04.113.
[22] H. Malekshah E., et al., Optimizing geometrical structure of a residential parabolic solar collector relying on hydrothermal assessment and second law analysis, Eng. Anal. Bound. Elem. 157 (2023) 314–325.
[23] N. Ullah, I. Sami, A. Jamal Babqi, I. Alkhammash, H., Y. Belkhier, A. Althobaiti, A. Ibeas, Processor in the loop verification of fault tolerant control for a three phase inverter in grid connected PV system, Energy Sour. Part A Recov. Util. Environ. Effects 45 (2) (2021) 3760–3776, https://doi.org/10.1080/15567036.2021.2015486.
[24] A. Althobaiti, N. Ullah, Y. Belkhier, A. Jamal Babqi, H.I. Alkhammash, A. Ibeas, Expert knowledge based proportional resonant controller for three phase inverter under abnormal grid conditions, Int. J. Green Energy 20 (7) (2022) 767–783, https://doi.org/10.1080/15435075.2022.2107395.
[25] Hamza Belmadani, Rafik Bradai, Aissa Kheldoun, Karam Khairullah Mohammed, Saad Mekhilef, Youcef Belkhier, Adel Oubelaid, A New Fast and Efficient MPPT Algorithm for Partially Shaded PV Systems Using a Hyperbolic Slime Mould Algorithm, 2024.
[26] Shunli Wang, Yongcun Fan, Siyu Jin, Paul Takyi-Aninakwa, Carlos Fernandez, Improved anti-noise adaptive long short-term memory neural network modeling for the robust remaining useful life prediction of lithium-ion batteries, Reliab. Eng. Syst. Saf. 230 (2023) 108920, https://doi.org/10.1016/j.ress.2022.108920.
[27] Shunli Wang, Paul Takyi-Aninakwa, Siyu Jin, Chunmei Yu, Carlos Fernandez, Daniel-Ioan Stroe, An improved feed forward-long short-term memory modeling method for the whole-life-cycle state of charge prediction of lithium-ion batteries considering current-voltage-temperature variation, Energy 254 (Part A) (2022) 124224, https://doi.org/10.1016/j.energy.2022.124224.
[28] K. Srilakshmi, A. Ramadevi, J.G.P. Reddy, K. Krishna Jyothi, K. Kondreddi, P. K. Balachandran, I. Colak, A new control scheme for wind/battery fed UPQC for the power quality enhancement: a hybrid technique, IETE J. Res. 1–9 (2024), https://doi.org/10.1080/03772063.2024.2370959.
[29] K. Srilakshmi, A.N. Pandian, A. Palanivelu, Fuzzy based hybrid controller for UPQC with wind and battery storage systems, Int. J. Electron. 1–26 (2023), https://doi.org/10.1080/00207217.2023.2245193.